Long Wave Models with Application to High Speed Vessels in Shallow Water

Philosophiae Doctor Thesis

Tomas Torsvik

Department of Mathematics
University of Bergen
Norway

December 2006

Preface

This thesis contains work that has been carried out as part of a Ph.D. program at the Department of Mathematics, University of Bergen, Norway. The studies started in July 2003, and I have conducted most of my work while in Bergen, except for an extended visit to Cornell University, Ithaca, USA, from September to December 2005.

My supervisors have been Prof. Kristian Dysthe at the Department of Mathematics, University of Bergen, and Prof. Geir Pedersen at the Department of Mathematics, University of Oslo. Funding has been provided by the Norwegian research council (NFR) within the program *Modeling of currents and waves for sea structures* (NFR 146526/420).

The main objective of this thesis has been to study wash from high speed vessels in shallow water, and the mathematical equations which describe this phenomenon. Several adverse effects can be related to wash from high speed vessels, and it is therefore important to understand the origin of these waves and how to avoid generation of large amplitude wash in sensitive areas.

Papers included in the thesis

The following papers are included in the thesis:

Paper A: Influence of Variable Froude Number on Waves Generated by Ships in Shallow Water. T. Torsvik, K. Dysthe, and G. Pedersen. In *Physics of Fluids*, volume **18**(6), 2006.

Paper B: Waves generated by a pressure disturbance moving in a channel with a variable cross section topography. T. Torsvik, K. Dysthe, and G. Pedersen. To be submitted.

Paper C: An Efficient Method for the Numerical Calculation of Viscous Effects on Transient Long-Waves. T. Torsvik and P. L.-F. Liu. Accepted for publication in *Coastal Engineering*.

Paper D: Stability Analysis of Geostrophic Adjustment on Hexagonal Grids for Regions with Variable Depth. T. Torsvik, Ø. Thiem, and J. Berntsen. In *Monthly Weather Review*, volume **133**, pp. 3335-3344, 2005.

As all the papers have been written in collaboration with other researchers, some remarks about my contributions are necessary.

Paper A explores the effect of a slowly changing Froude number, either caused by acceleration of the pressure disturbance or by depth variation. All the authors were involved in developing the basic concept for this paper. My contribution

included reviewing the existing literature on effects due to a variable Froude number, and implementing a finite difference scheme for solving the equations. I have had the main responsibility for writing the paper, with helpful comments and suggestions from my supervisors. Paper B explores the effect of cross channel depth variation, where a ship travels along a trench which runs along the center line of the channel, and shallow banks are located near the channel walls. For this paper we applied the COULWAVE model for the simulations. The paper was created in a manner similar to paper A, where all the authors were involved in developing the basic concept for the paper, and I, as principle author, was responsible for writing the paper. My contribution also included modifying some aspects of the COULWAVE model, thereby making it suitable to use for the problem at hand, and also involved calculating solutions for the channel width averaged model applied for comparison. Paper C presents an efficient method for calculating the viscous effects due to bottom friction, by estimating the value of a time dependent convolution integral. My contribution included method development, in collaboration with Prof. Philip L.-F. Liu, and implementation for this estimate for the COULWAVE model. I have written the paper, while Prof. Liu has contributed with useful suggestions and comments. Paper D presents a method for analyzing the stability of a numerical finite difference scheme for the linearized shallow water equations, formulated on a hexagonal grid. My contribution consisted of developing model equations on the hexagonal grid, and analyzing some of the idealized test cases (three-cell and nine-cell computational domains). All of the authors contributed in the writing of this paper.

Acknowledgements

I must first of all thank my supervisors Prof. Kristian Dysthe at the Department of Mathematics, University of Bergen, and Prof. Geir Pedersen at the Department of Mathematics, University of Oslo, for their substantial contribution to this thesis. Their contribution involve both overall guidance on fruitful lines of investigation and general requirements for scientific work, as well as contribution on specific numerical and mathematical problems we have encountered along the way. In addition to their contribution as supervisors, they have also contributed as co-authors on two of the papers presented in this thesis.

I would also like to thank the other co-authors I have had the pleasure of working with during my Ph.D., Prof. Philip L.-F. Liu at the School of Civil and Environmental Engineering, Cornell University, USA, Prof. Jarle Berntsen at the Department of Mathematics, University of Bergen, and Dr. Øyvind Thiem, who is now working at the Computational Mathematics Unit, Bergen Center for Computational Studies. The work on hexagonal grids which is part of paper D was

originally done as part of a course in ocean modeling, and I am grateful to Prof. Jarle Berntsen for introducing me to this topic and for all his help in writing the paper. I am especially grateful to Prof. Philip L.-F. Liu for having me as a guest student at Cornell University during the fall 2005.

I am indebted to Prof. John Grue who headed and obtained the funding for the project "modeling of currents and waves for sea structures", and thereby provided me with the funding I needed to complete my Ph.D. study.

I would like to thank Dr. Patrick Lynett at Coastal and Ocean Engineering, Texas A&M, for providing me with an updated version of the COULWAVE model. I am indebted to Dr. Tso-Ren Wu at the Institute of Hydrological Sciences, National Central University, Taiwan, who assisted me with the model, and in particular with how to include an external pressure disturbance, and to Dr. Alejandro Orfila for allowing me to use his model for calculating the bottom drag, which I used for comparison in one of the papers.

I would like to thank my fellow students at the Department of Mathematics, without whom everyday life at the department would be far less enjoyable. As a Ph.D. student it is easy to become tangled up in the details of ones own studies, so I have found it very helpful to have people around me who could distract me in a most positive way.

Finally, I would like to thank my family for their support and encouragement during my years of study.

Tomas Torsvik
Bergen, December 2006.

Contents

Part I

Introduction

Chapter 1

Wash from high speed vessels: Basic properties and potential risks

During the last few decades, several ferry operators have replaced conventional ships with High Speed Crafts (HSCs) for transporting passengers and vehicles, and the number of these crafts in operation is steadily increasing. Replacing conventional ferries with HSCs often requires new regulations from harbor authorities to ensure safe passage in near-shore regions. Among the issue which must be addressed, is how to manage the increased wave load due to wash waves from a HSC compared to wash from conventional ships. While the wash waves from conventional ships transport energy on scales similar to typical wind waves, HSCs often generate highly energetic long period waves which differ significantly from the typical waves found in confined bodies of water.

1.1 High speed vessels and wash waves

The wash waves generated by a particular vessel in a particular body of water are characterized in terms of the length-based Froude number $F_L = U/\sqrt{gL_w}$, and the depth-based Froude number $F_h = U/\sqrt{gh}$, where U is the speed of the ship, L_w is the length of the ship at the water line, g is the acceleration of gravity and h is the depth. Although the Froude numbers provide a convenient method for the purpose of classification, other factors such as the shape of the hull, the type of propulsion system, and the variation in bathymetry will also influence the wash.

There is no precise definition for classifying a vessel as a HSC. According to Faltinsen[1], a common demarcation for a HSC is vessel capable of operating at speeds higher than 30 knots or with a length-based Froude number F_L above 0.4. Vessels operating at $F_L < 0.4$ are called displacement vessels, because they are mainly supported by the buoyancy force which is proportional to the submerged volume of the ship. At $F_L = 1.0 - 1.2$, most of the weight of the ship is carried by the hydrodynamic pressure, and the vessel is said to be planing. If a vessel has its maximum operational speed in the intermediate range $0.4 - 0.5 < F_L < 1.0 - 1.2$, it is classified as a semi-displacement vessel.

Several different designs are used for HSCs, of which there are three main categories; submerged hull-supported vessels, Hydrofoil-supported vessels and air cushion-supported vessels. Some designs may apply a combination of these technologies, such as the Surface Effect Ship (SES) which combines a catamaran design with an air cushion enclosed between the two hulls. An overview of common designs can be found in Faltinsen[1]. Large HSCs, which are semi-displacement vessels, are usually designed as catamarans or monohulls.

The wake of a ship consists of a transverse wave group directed along the ship's track, and a divergent wave group propagating at an angle to the track, as sketched in figure 1.1. Waves generated by a ship traveling in deep water or at low speeds in shallow water, form a Kelvin ship-wave pattern. The angle between

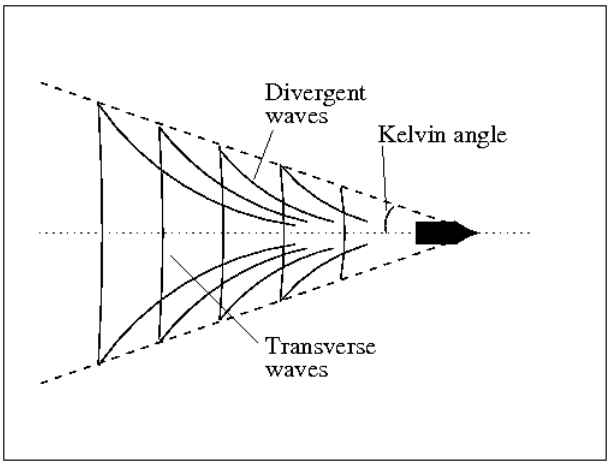

Figure 1.1: Wave crests for the Kelvin ship-wave pattern.

the boundary of the wave system and the ship's track, which is called the Kelvin angle, is $19°28'$ for the deep water wave pattern. Because the wake waves are stationary in a coordinate system following the vessel (moving along a straight line with constant speed), the wavelength is expressed by

$$\lambda = \frac{U^2}{g} 2\pi \cos^2\theta,$$

where θ is the direction of the wave propagation relative to the course of the ship. For the transverse waves we have

$$\frac{\lambda_T}{L} = 2\pi {F_L}^2.$$

When the length-based Froude number is $0.4-0.5$ (often called the "hump-speed"), waves originating at the bow and stern of the ship may interact to cause wave amplification or cancellation in the wake. This will in turn contribute to humps and hollows in the wave resistance when plotted as a function of F_L. When F_L becomes larger than $0.6-0.7$, the divergent waves tend to dominate the wave pattern, and the humps and hollows in the wave resistance disappear. From a coastal management perspective, the primary interest with respect to the wash waves concerns the impact of these waves on shore lines or in relation to other users of the coastal region. Hence the sites of interest may be located a considerable distance from the track of the HSC generating the wash, and the wash waves may decay significantly as they propagate over this distance. The problem of wave decay has been analyzed by Stoker[2] for a ship moving along a straight line in a water basin of constant depth. Stoker[2] showed by use of linear analysis, that the waves in the interior of the wedge created by the Kelvin wake pattern, decay

as $|y|^{-1/2}$, where y is the direction perpendicular to the track of the ship, whereas the rate of decay for the waves on the boundary of the wedge is $|y|^{-1/3}$.

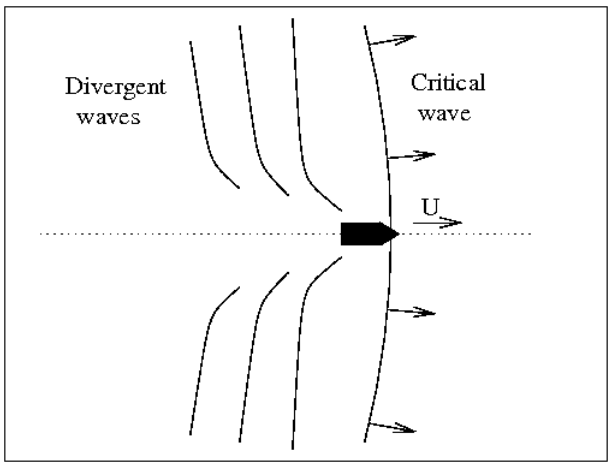

Figure 1.2: Wave crests for wash generated near the critical depth-based Froude number $F_h \approx 1$.

The wave pattern generated in the wake of the ship changes in intermediate or shallow water, where the value of the depth Froude number F_h may become large. The deep water description of the wash is valid up to $F_h \lesssim 0.5 - 0.6$. As F_h approaches 1, the Kelvin angle increases and becomes 90° in the limit $F_h = 1.0$. A sketch of the near critical wash waves is shown in figure 1.2. At $F_h \approx 1.0$, the ship is continually contributing energy to a wave group which is moving at the same speed as the vessel, resulting in the generation of large amplitude waves, which in turn contributes to an increase in the wave resistance against the forward movement of the ship. Due to nonlinear effects, one or more waves originating at the bow of the ship may propagate some distance upstream of the vessel. If the water basin is enclosed by lateral walls, such as in a channel, the upstream waves may evolve into a train of solitary waves which becomes separated from the wave-system of the ship. When the depth Froude number is supercritical ($F_h > 1.0$), the Kelvin angle becomes smaller than 90°, and the wake of the ship consists only of divergent waves. Because the ship travels at a higher speed than the maximum (linear) wave speed, there can be no transverse waves in the wake once this has reached a steady state.

The decay of the wash waves in intermediate and shallow water is discussed in Doyle et al.[3]. Wash wave amplitudes decay at different rates depending on the depth Froude number F_h and the water depth-to-ship length ratio h/L_w, ranging from $|y|^{-0.2}$ to $|y|^{-0.5}$. The decay rate is larger for wash generated in the near critical range $F_h \approx 1$, than in the supercritical range $F_h \gg 1$, and decrease with

decreasing values of h/L_w. It has however been shown that the decay rate of the leading wave system at $F_h \approx 1$ decreases with time. In the critical case, most of the wave energy is contained in a wave group which is moving with the vessel. Since the amplitude of these waves can not grow indefinitely, an increasing amount of energy will have to be transferred in the lateral direction along the crest. It is reasonable to expect that a state of equilibrium will be attained after a long time, where the input of energy is equal to the energy transferred along the crest, but this has so far not been confirmed in experiments.

The forward motion of the vessel is influenced by the wave resistance due to wash wave generation. The wave resistance depends primarily on the velocity of the vessel and the shape of the submerged part of the ship, but is also influenced by the depth of the water basin (the basic theory is covered in Newman[4]). Yang[5] computed the ratio of the wave resistance in shallow water R_h with the wave resistance in deep water R_∞, using linear theory. Near the critical depth Froude number $F_h \approx 1$, it was found that $R_h/R_\infty > 3$ for $h/L_w \approx 0.2$, and even larger values for R_h/R_∞ were recorded for smaller values of h/L_w. It is however questionable if the linear theory is applicable in the limit $h/L_w \to 0$, because the shallow water waves are influenced by nonlinear effects when $F_h \approx 1$. It was also found that $R_h/R_\infty \approx 1$ for $h/L_w \gtrsim 0.4$ (and $F_h \approx 1.0$), which corresponds to $F_L > 0.6$. A similar result was found by Stumbo et al.[6] through full-scale measurements, although in their study, wave amplitudes were reduced for $F_L > 0.9$. In the supercritical region, the ratio R_h/R_∞ diminish and is approximately 1 for all values of h/L_w when $F_h > 1.8$.

1.2 Problems and responses

When HSCs first started replacing conventional ships on ferry routes, coastal authorities were concerned mainly with ensuring safe navigation in order to prevent collisions and grounding accidents, while possible problems due to the wake waves were largely ignored. The wash from conventional ferries are not usually considered a hazard, and thus there had been no incentive for regulating ship wash prior to the commencement of HSC ferry operations. In several cases, some of which are listed in [7], the commencement of HSC ferry traffic was followed by an increase in wash related incidents with damage on people or property, especially in cases where the HSC traveled in or near coastal waters not exposed to ocean swell. Coastal authorities would often respond by setting speed limits for HSC operation in regions which were particularly vulnerable to wash waves. Because the nature of the problem was not well understood, the speed limits would often be lower than necessary, reducing the profitability of the HSC ferry operation. In some cases the speed limit would make the HSC move in an unfavorable speed regime, thus aggravating the problem which the speed limit was intended

to solve, as seen in the case of Stavns Fjord, Samsø in Denmark[7]. In this case the fast ferry was allowed to operate at a service speed of approximately 35 knots (18 m/s), but was restricted to a maximum speed of 25 knots (13 m/s) during the summer months. As the length of the vessel was about 78 m and the typical depth was 15 meters, the speed reduction caused the vessel to move at Froude numbers $F_L \approx 0.47$ and $F_h \approx 1.06$. When it became apparent that the speed reduction did not reduce the height of the wash waves, the speed was reduced once again to 18 knots. It is now widely recognized that regulations related to wash waves must set limits to actual wave heights and periods.

Ship wash may constitute a safety hazard or have an adverse effect on the coastal environment. Safety issues include the possible risk to people at the shore or in small boats, who are exposed to wash waves. The amplitude of the waves increase as they propagate into shallow water, and large amplitude waves may therefor occur unexpectedly at the shore or near shallow banks. A well documented case occurred in 1999, when the angling boat "Purdy" was swamped by wash from a HSC at Shipwash Bank off Harwich, UK[8]. In this case, wave focusing due to maneuvers from the HSC may have contributed to the accident. Other safety issues include damage to structures near the shore, or breaking of mooring lines. Environmental issues include the alteration of the shore line due to increased erosion, alteration of the near-shore bathymetry, suspension of sediments for long periods of time, and the impact of wash waves on marine wildlife habitats. These problems may occur even in regions which are not sheltered from wind driven waves, as discussed by Soomere[9], because the long periods of the wash waves induces stronger bottom currents than the shorter period wind driven waves.

In order to minimize the adverse effects of wash waves, detailed planning of ship routs and speed regulations must be conducted prior to commencement of HSC operation. This involves testing the particular HSC design for wash characteristics at different speeds and depths, and constructing new vessels which emit low wash. It also involves predicting how the waves evolve when subject to speed changes and maneuvers by the ship, and depth variation as the waves propagates away from the ship lane. Stumbo et al.[10] reports that the Washington State Ferries operate with a "no harm" level of wake wash which is established by examining the wash generated by the HSC in deep water, based on the requirement that the energy associated with the wash should not exceed levels associated with other sources. Sweden and Denmark have implemented a criteria based on the wave height close to shore[7]. While this my be more difficult to assess than the offshore wave height, it has the advantage of being weighted toward the shoreline where the adverse effects are most likely to occur. Even if the HSC generates waves within an acceptable range of wave height, wave interactions may create dangerous wash in regions some distance away from the ship lane. Wave mod-

els can be useful tool for identifying mechanisms which may create large wash in general cases, and can also be used to predict likely wash effects in particular water basins without conducting potentially harmful field tests. The two first papers in this thesis, A and B, contribute to this field of research. In paper A we consider how the wash is influenced when the Froude number changes with time, which is caused either by acceleration of the HSC or a slow variation in the bathymetry. Paper B treats the problem of wash generated by a vessel moving in a channel with shallow banks near the channel walls. Although both these studies are based on idealized benchmark tests, the cases studied resemble some of the practical problems which must be considered when predicting HSC wash in coastal regions.

Chapter 2

Equations for ship generated long waves

In this chapter we will consider equations which can be used to describe the wash from a HSC in intermediate to shallow water. As mentioned in chapter 1, the dominating waves in the ship wake pattern often have wave lengths comparable to or exceeding the length of the ship. In regions of shallow water, where the longest wave length in the wash may be considerably larger than the depth, these waves can be described accurately by long wave equations. In long wave theory, the vertical distribution of the flow field is approximated by a polynomial expression. By using this approximation, we can eliminate the vertical coordinate z in the partial differential equations, effectively reducing the three dimensional flow problem to a two dimensional flow problem.

Based on the different length scales which occur in the problem, it is possible to construct two non-dimensional parameters. The ratio of depth to wave length, μ, governs linear dispersion, and nonlinear effects are governed by the ratio of wave amplitude to depth, ε. Very long waves are non-dispersive, and disregarding terms of $O(\mu)$ gives us the *shallow water equations*, which can be used if the water depth is less than 7% of the wavelength (see e.g. Kundu[11]). Less restrictive equations, such as the *standard Boussinesq equations* and the *Korteweg-de Vries equation*, can be derived if we assume that the waves are weakly dispersive and weakly nonlinear, i.e. that $O(\varepsilon) = O(\mu^2) \ll 1$. These equations are practical for use in large scale computations of processes in the coastal region, but they are still limited to describing fairly long waves with small amplitudes. Much effort has gone into improving the dispersive and nonlinear properties of the Boussinesq equations, with the intention of applying these formulations to processes such as wave shoaling and run-up, refraction and diffraction near a step in the bottom topography, etc. With improved formulations, it is possible to describe accurately waves with wave numbers up to $k'h' \approx 6$. These formulations provides accurate results for linear shoaling characteristics over a wide range of depths. Highly nonlinear processes, such as wave breaking, are not represented accurately, but can be accounted for with the aid of empirical remedies (see e.g. Kennedy et al.[12]).

2.1 Primitive equations

The fluid in the physical domain is described by the fluid velocity $\mathbf{u}' = (u', v', w')$, the free surface displacement $z' = \zeta'(x', y', t')$, and the bottom $z' = -h'(x', y')$. In order to distinguish between variables with and without dimensions, primes are used on dimensional variables whenever there is a possibility of confusion. The fluid is assumed to be incompressible, with constant density ρ, and irrational in the core region away from solid boundaries. Forces acting on the fluid are pressure p' and gravity with acceleration g. With these assumptions, waves propagation on

the air-sea interface can be described by the continuity and Euler equations

$$\nabla_o \cdot \mathbf{u}' = 0\,, \tag{2.1}$$

$$\frac{\partial \mathbf{u}'}{\partial t} + (\mathbf{u}' \cdot \nabla_o)\mathbf{u}' + \frac{\nabla_o p'}{\rho} + g\nabla_o z' = 0\,, \tag{2.2}$$

with the boundary conditions

$$w' = \frac{\partial \zeta'}{\partial t'} + u'\frac{\partial \zeta'}{\partial x'} + v'\frac{\partial \zeta'}{\partial y'}\,, \quad \text{at} \quad z' = \zeta'(x',y',t')\,, \tag{2.3}$$

$$p' = p_a(x',y',t')\,, \quad \text{at} \quad z' = \zeta'(x',y',t')\,, \tag{2.4}$$

$$w' + u'\frac{\partial h'}{\partial x'} + v'\frac{\partial h'}{\partial y'} = 0\,, \quad \text{at} \quad z' = -h'(x',y')\,, \tag{2.5}$$

for the free surface and the bottom, where

$$\nabla_o = \left(\frac{\partial}{\partial x'}, \frac{\partial}{\partial y'}, \frac{\partial}{\partial z'}\right)$$

is the gradient operator in three dimensions.

When we consider long waves propagating in shallow water, we can use the differences in length scales given by a typical wave amplitude a_0, the typical water depth h_0, and a typical horizontal length scale h_0, to derive equations which are easier to solve than the original set (2.1) to (2.5). These length scales define the parameters

$$\varepsilon = \frac{a_0}{h_0}\,, \quad \text{and} \quad \mu = \frac{h_0}{l_0}\,, \tag{2.6}$$

which govern nonlinear and dispersive effects, respectively. When deriving the Boussinesq equations, it is customary to use non-dimensional variables which are scaled according to

$$\begin{aligned} (x,y) &= \frac{(x',y')}{l_0}\,, \qquad z = \frac{z'}{h_0}\,, \qquad h = \frac{h'}{h_0}\,, \qquad t = \frac{\sqrt{gh_0}}{l_0}t'\,, \\ (u,v) &= \frac{(u',v')}{\varepsilon\sqrt{gh_0}}\,, \qquad w = \frac{\mu w'}{\varepsilon\sqrt{gh_0}}\,, \qquad \zeta = \frac{\zeta'}{a_0}\,, \qquad p = \frac{p'}{\rho g a_0}\,. \end{aligned} \tag{2.7}$$

Although this is convenient when discussing the equations, using different length scales for different variables obscures output from numerical simulations. For numerical studies it is therefore customary to formulate the equations using only the typical depth h_0 as the reference length scale.

Boussinesq equations can be formulated in several different ways, depending on the choice of dependent variables and the order of the equations. The equations

are usually derived by depth-integrating the continuity and Euler equations (see e.g. Peregrine[13], Nwogu[14]), or by formulating the equations in terms of the velocity potential, and use the Laplace equation in combination with the boundary conditions (see e.g. Mei[15]). An outline of the derivation following Madsen and Schäffer[16] is given in appendix A.1.

2.2 Boussinesq equations

The fully nonlinear Boussinesq equations of order $O(\mu^2)$, can be written as

$$\frac{\partial \zeta}{\partial t} = -\nabla \cdot \left[(h+\varepsilon\zeta)(\mathbf{u}+\mu^2\mathbf{M}\right] + O(\mu^4)\,, \tag{2.8}$$

$$\begin{aligned}\frac{\partial \mathbf{u}}{\partial t} + \frac{\varepsilon}{2}\nabla(\mathbf{u}^2) = -\nabla\zeta - \nabla p - \mu^2 \left[\frac{1}{2}z_\alpha^2 \nabla\nabla\cdot\frac{\partial \mathbf{u}}{\partial t} + z_\alpha \nabla\nabla\cdot\left(h\frac{\partial \mathbf{u}}{\partial t}\right)\right] \\ + \varepsilon\mu^2\nabla(D_1+\varepsilon D_2+\varepsilon^2 D_3) + O(\mu^4)\,,\end{aligned} \tag{2.9}$$

where

$$\begin{aligned}\mathbf{M} &= \left[\frac{1}{2}z_\alpha^2 - \frac{1}{6}(h^2 - \varepsilon h\zeta + \varepsilon^2\zeta^2)\right]\nabla\nabla\cdot\mathbf{u} + \left[z_\alpha + \frac{1}{2}(h-\varepsilon\zeta)\right]\nabla\nabla\cdot(h\mathbf{u})\,,\\
D_1 &= \zeta\nabla\cdot\left(h\frac{\partial \mathbf{u}}{\partial t}\right) - \frac{1}{2}z_\alpha^2\mathbf{u}\cdot\nabla\nabla\cdot\mathbf{u} - z_\alpha\mathbf{u}\cdot\nabla\nabla\cdot(h\mathbf{u}) - \frac{1}{2}(\nabla\cdot(h\mathbf{u}))^2\,,\\
D_2 &= \frac{1}{2}\zeta^2\nabla\cdot\frac{\partial \mathbf{u}}{\partial t} + \zeta\mathbf{u}\nabla\nabla\cdot(h\mathbf{u}) - \zeta\nabla\cdot(h\mathbf{u})\nabla\cdot\mathbf{u}\,,\\
D_3 &= \frac{1}{2}\zeta^2\left[\mathbf{u}\cdot\nabla\nabla\cdot\mathbf{u} - (\nabla\cdot\mathbf{u})^2\right].\end{aligned}$$

In these equations $\nabla = (\partial/\partial x, \partial/\partial y)$ is the gradient operator in two dimensions, and the velocity $\mathbf{u}$ is evaluated at the depth $z = z_\alpha$. We have retained the ambient surface pressure in the momentum equation (2.9), which will serve as a forcing term in the model for ship generated waves. The equations (2.8) and (2.9) correspond to the equations used in paper B.

The so-called classical or standard Boussinesq equations is often formulated in terms of the averaged horizontal velocity $\bar{\mathbf{u}}$, which can be defined in terms of the integrated, horizontal volume flux density $\mathbf{Q}$ by

$$\mathbf{Q} = (h+\varepsilon\zeta)\bar{\mathbf{u}}\,.$$

From the requirement of volume conservation, which can be formulated by integrating the continuity equation over the depth, we find

$$\frac{\partial \zeta}{\partial t} = -\nabla\cdot\mathbf{Q}\,,$$

which, formulated in terms of the averaged horizontal velocity, gives us

$$\frac{\partial \zeta}{\partial t} + \nabla \cdot [(h + \varepsilon\zeta)\bar{\mathbf{u}}] = 0\,. \tag{2.10}$$

This equation is consistent with (2.8) if we define $\bar{\mathbf{u}} = \mathbf{u} + \mu^2\mathbf{M}$, and retain only terms up to $O(\mu^2, \varepsilon)$. Substituting this into the momentum equation (2.9), we find

$$\begin{aligned}\frac{\partial \bar{\mathbf{u}}}{\partial t} + \varepsilon(\bar{\mathbf{u}} \cdot \nabla)\bar{\mathbf{u}} = &-\nabla\zeta - \nabla p \\ &- \mu^2 \left[\frac{1}{6}h^2\nabla\nabla \cdot \frac{\partial \bar{\mathbf{u}}}{\partial t} - \frac{1}{2}h\nabla\nabla \cdot \left(h\frac{\partial \bar{\mathbf{u}}}{\partial t}\right)\right] + O(\mu^4, \mu^2\varepsilon)\,.\end{aligned} \tag{2.11}$$

Equations (2.10) and (2.11) constitute the *standard Boussinesq equations*.

The formulations for the Boussinesq equations stated above are valid for rotational flow. If the flow can be assumed irrotational, it is possible to reduce the number of unknowns by introducing the velocity potential Φ, and formulate the equations in terms of the depth averaged velocity potential

$$\phi = \frac{1}{h + \varepsilon\zeta}\int_{-h}^{\varepsilon\zeta} \Phi\, dz\,.$$

The relation between the averaged horizontal velocity and the depth averaged velocity potential is given by (see e.g. Wu[17], Pedersen[18])

$$\bar{\mathbf{u}} = \nabla\phi + \mu^2\left(\frac{1}{6}\frac{\partial \zeta}{\partial t} - \frac{1}{3}\nabla h \cdot \nabla\phi\right)\nabla h + O(\mu^4, \mu^2, \varepsilon)\,,$$

which can be substituted into (2.10) and (2.11), to give us the the standard Boussinesq equations on the form

$$\frac{\partial \zeta}{\partial t} + \nabla \cdot \left[(h + \varepsilon\zeta)\nabla\phi + \mu^2 h\left(\frac{1}{6}\frac{\partial \zeta}{\partial t} - \frac{1}{3}\nabla h \cdot \nabla\phi\right)\nabla h\right] = 0\,, \tag{2.12}$$

$$\begin{aligned}\frac{\partial \phi}{\partial t} + \frac{1}{2}\varepsilon(\nabla\phi)^2 = &-\zeta - p \\ &- \mu^2 \left[\frac{1}{6}h^2\nabla\nabla \cdot \frac{\partial \phi}{\partial t} - \frac{1}{2}h\nabla \cdot \left(h\nabla\frac{\partial \phi}{\partial t}\right)\right] + O(\mu^4, \mu^2\varepsilon)\,.\end{aligned} \tag{2.13}$$

Equations (2.12) and (2.13) are equivalent to the equations used in Paper A.

2.2.1 The Korteweg-de Vries equation

The Korteweg-de Vries (KdV) equation

$$\frac{\partial \zeta}{\partial t} - \left(1 + \frac{3}{2}\varepsilon\zeta\right)\frac{\partial \zeta}{\partial x} - \frac{1}{6}\mu^2\frac{\partial^3 \zeta}{\partial x^3} = \frac{1}{2}\frac{\partial p}{\partial x}, \tag{2.14}$$

can be derived from the standard Boussinesq equations by restricting the flow to one horizontal dimension (1HD) and imposing that the flow moves in one direction only (see e.g. Lee et a.[19]). In equation (2.14) we have assumed that the depth is constant, which we may choose as $h = 1$ without loss of generality. Although this equations has a smaller range of validity than the Boussinesq equations in terms of wave lengths and amplitudes, it is nevertheless quite popular because it can be solved analytically by applying the so-called *inverse scattering transform* (see e.g. Drazin and Johnson[20]).

2.2.2 Analysis of Boussinesq type equations

In order to classify the accuracy of the different formulations of the Boussinesq equations, it is common to examine the equations in relation to the linear dispersion characteristics of the primitive equations, and to apply a Stokes-type perturbation analysis to examine nonlinear properties. In this section we examine the dispersion relation for the equations presented in the previous section. Nonlinear properties are not examined here, but properties for equivalent formulations of the equations can be found in the review paper by Madsen and Schäffer[16].

In order to improve the performance of the Boussinesq equations for intermediate wave lengths and depths, it is customary to examine the evolution of a linear wave solution, using linearized versions of the Boussinesq equations. The aim is to approximate the exact dispersion relation for the linear waves, given by

$$c^2 = \frac{\omega^2}{k^2} = \frac{\tanh(kh)}{kh}, \tag{2.15}$$

as accurately as possible. This equation gives us the Taylor expansion approximation

$$c^2 = 1 - \frac{1}{3}(kh)^2 + \frac{2}{15}(kh)^4 + O((kh)^6). \tag{2.16}$$

The corresponding Padé [2,2] approximation is

$$c^2 = \frac{1 + \frac{1}{15}(kh)^2}{1 + \frac{2}{5}(kh)^2} + O((kh)^6). \tag{2.17}$$

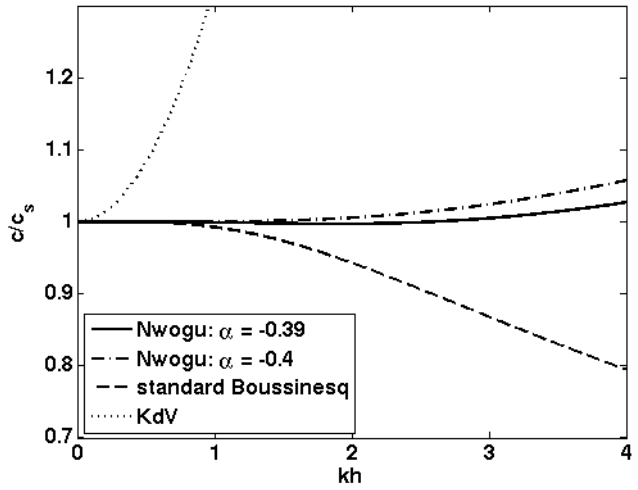

Figure 2.1: Dispersion relation for different formulations of the Boussinesq equations.

The dispersion properties of the equations can be studied by assuming wave solutions on the form

$$\zeta = a_0 e^{i(kx-\omega t)}, \quad u = u_0 e^{i(kx-\omega t)}, \quad \phi = \phi_0 e^{i(kx-\omega t)},$$

and substituting these expressions into the linearized Boussinesq and KdV equations. The dispersion relations for the linearized KdV equation (from (2.14)) and the linearized standard Boussinesq equations (from (2.10) and (2.11)) are

$$c^2 = 1 - \tfrac{1}{3}(hk)^2, \quad \text{and} \quad c^2 = \frac{1}{1+\frac{1}{3}(hk)^2},$$

respectively. The dispersion relation for the KdV equation is equal to the first terms of the Taylor expansion in equation (2.16). The fully nonlinear Boussinesq equations ((2.8) and (2.9)) reduces to Nwogu's equations[14] when linearized, with the dispersion relation

$$c^2 = \frac{1-(\alpha+\frac{1}{3})(hk)^2}{1-\alpha(hk)^2},$$

where α depends on the reference depth z_α

$$\alpha = \frac{1}{2}\frac{z_\alpha^2}{h^2} + \frac{z_\alpha}{h}.$$

The Padé [2,2] approximation (2.17) is recovered by choosing $\alpha = -0.4$. We can now compare the dispersive properties for the different equations by comparing

the above results to the dispersion relation for the linear wave 2.15 with phase speed c_s, as shown in figure 2.1. As seen in the figure, $\alpha = -0.390$ gives an approximation which is good up to $kh \approx 3$. This value of α corresponds to $z_\alpha/h = -0.531$.

The techniques discussed so far in this section are used to determine general properties of the Boussinesq equations. It may also be useful to analyze the equations for more specific problems. Perturbation techniques can be used to analyze linear shoaling characteristics and dispersion characteristics for waves influenced by an ambient current, as shown by Madsen and Schäffer[16]. Løvholt and Pedersen[21] have examined the stability of Boussinesq models for regions of non-uniform depth by analyzing the eigenmodes of the equations given a specific depth profile, using a combination of analytical and numerical methods. While the standard Boussinesq equations (2.10) and (2.11) were found to have only stable eigenmodes, other formulations would sometimes have unstable modes, especially for small spatial grid increments and steep bottom gradients.

2.3 Channel width integrated model equations

For wave analysis purposes it is sometimes convenient to examine a simplified set of model equations. One such simplification is to consider only one spatial dimension, as in paper A, but this may be too restrictive for many purposes. A less restrictive option is to use cross-channel averaged model equations, which are derived under the assumption that the waves are long compared to the channel width. Such models were first studied by Peters[22] and Peregrine[23, 24], and has later been used by Teng and Wu[25, 26, 27]. The equations, which may be of Boussinesq or KdV type, resemble the standard formulations, but include a *shape factor* κ^2 which is determined by the channel geometry. The *channel Boussinesq equations* (cB) for a channel of width $2b$ at $z = 0$, and a channel cross section area A_0, is given by

$$\begin{aligned} 2b\frac{\partial\tilde{\zeta}}{\partial t} + \frac{\partial}{\partial x}\left[2b(\tilde{h}+\tilde{\zeta})\bar{u}\right] &= 0\,, \\ \frac{\partial\bar{u}}{\partial t} + \bar{u}\frac{\partial\bar{u}}{\partial x} + \frac{\partial\tilde{\zeta}}{\partial x} - \frac{1}{3}\kappa^2\tilde{h}^2\frac{\partial^3\bar{u}}{\partial x^2\partial t} &= -\frac{\partial\tilde{p}_a}{\partial x}\,, \end{aligned}$$

where the tildes and bars signify width averages and cross section averages, given by

$$\tilde{(\cdot)} = \frac{1}{2b}\int_{-b}^{b}(\cdot)\,dy, \quad \text{and} \quad \bar{(\cdot)} = \frac{1}{A_0}\iint_{A_0}(\cdot)\,dy\,dz,$$

respectively. Analytical solutions based on cB equations are used for comparison in paper B, and the procedure for determining κ^2 is briefly outlined in the appendix in that paper. The cross channel profile of the wave can be obtained as a perturbation of the cross-channel averaged surface elevation[25, 27].

2.3.1 Solitary waves propagating in a channel with a dredged trench along the center line

In paper B we compare a wave generated by a pressure disturbance to a solution of the cB equations. This section presents a comparison of the solitary wave simulated with the COULWAVE model, and the corresponding solitary wave solution for the cB equations. The cross section configuration is similar to the configuration used in paper B, with a trench extending from $y = 0$ to $y = 4$ and shallow banks extending from $y = 6$ to $y = 10$. For each test case, a suitable value for the depth variation was chosen while the mean depth was maintained at $h = 1$, and the depths in the trench and at the shallow bank was adjusted accordingly. The figures show two results for $\Delta h = 0.2$, with wave amplitudes $a = 0.0951$ and $a = 0.1850$, and a result for $\Delta h = 1.0$ and $a = 0.0818$. The figures clearly show good agreement between the results for the long waves, even when the depth variation is quite severe, while larger discrepancies are seen between the results for the large amplitude wave.

2.4 Ships in numerical models

In our models, we have used a disturbance in the ambient surface pressure to represent the ship. This is a convenient choice when using the Boussinesq equations, because it does not involve any additional model for dealing with the ship motion. Representing the ship by a pressure disturbance is acceptable for general case studies, such as the test cases in Papers A, B and C. While a ship hull may easily be ascribed to a particular pressure disturbance by letting the hull be determined by the surface depression (provided the wave pattern has attained a steady state), the inverse problem of ascribing a pressure disturbance to a particular hull shape is difficult (see e.g. Tuck et al.[28]). Accurate models for ship wash are available, but are often computationally demanding, making them unsuitable for studies which requires large computational domains. This has lead some researchers to consider combining accurate near ship models with an efficient shallow water wave model for waves far from the ship.

The thin ship theory by Michell[29] is often used to predict the wash generated by a ship. The ship is represented by point sources distributed on the center plane of the ship, where the sources are proportional to the longitudinal change in

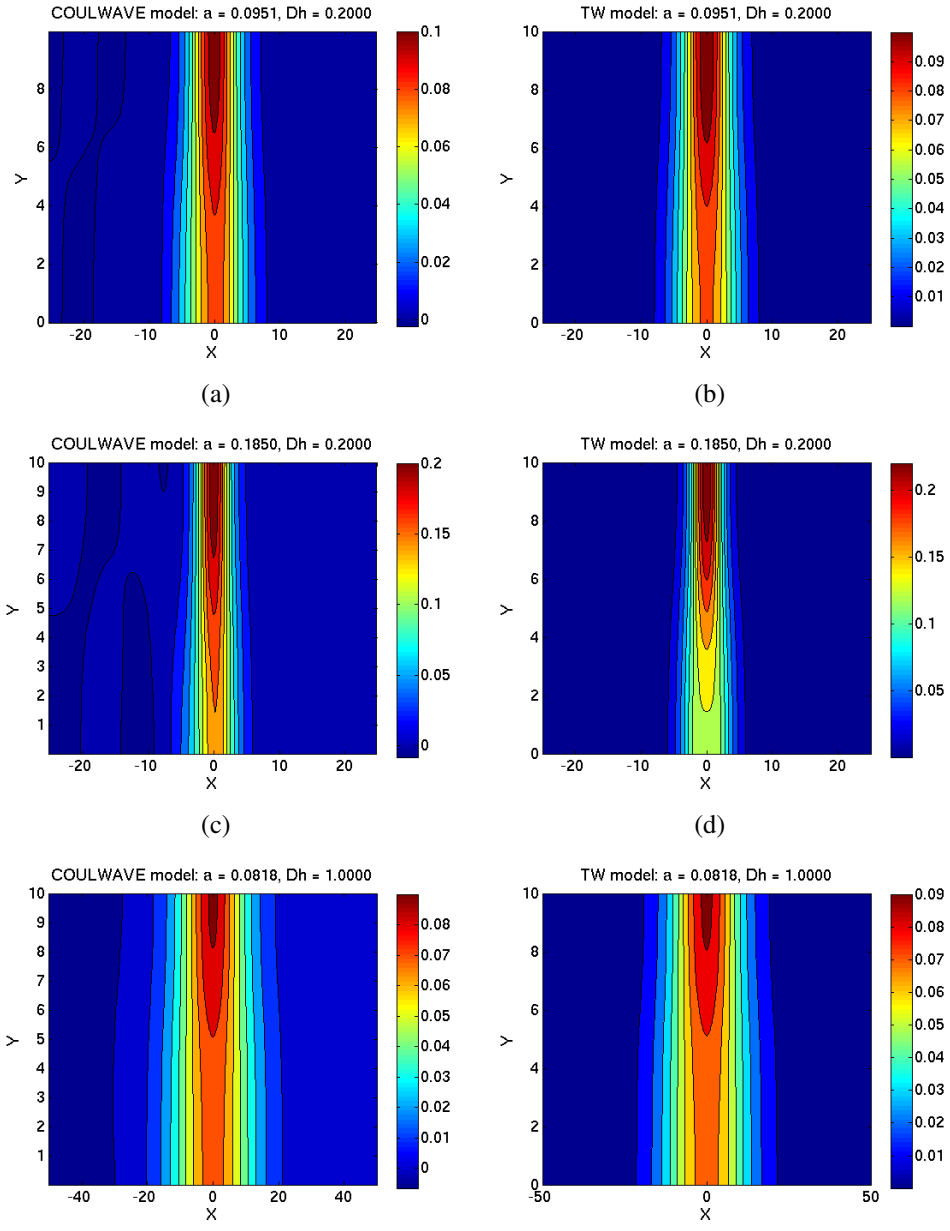

Figure 2.2: Surface plot of solitary waves propagating in a channel with a deep trench along the center line. The plots (a), (c), and (e) are from simulations with the COULWAVE model, whereas plots (b), (d), and (f) are the corresponding results using the cB model.

thickness of the hull. Thin ship theory has been applied to calculate HSC wash (see Tuck et al.[28]), but can only be used in cases where the wave field is steady and the wave amplitudes are small compared to the depth. Unsteady wave patterns and large wave amplitudes are often found in near critical cases, hence thin ship theory may not be applicable for $F_h \approx 1$. Tuck[30] examined the shallow water flow around a slender body, by matching asymptotic approximations for the flow near and far from the body. The expansions are written in terms of the *slenderness parameter* $\delta = R/L$, where R is the maximum lateral dimension and L is the length of the ship, and the depth is assumed to be $h = O(\delta)$. In the outer region, far from the ship, equations for shallow water waves are recovered, while equations for the inner region are derived under the assumptions that the flow varies much faster across the boundary layer than along the layer, i.e. $\partial/\partial x \ll \partial/\partial y, \partial/\partial z$ (see Tuck[30], Newman[4] for a complete description of the method). From the inner problem we get a matching condition by taking the limit $y/\delta \to \infty$, which must be satisfied by the outer flow in a matching region. This matching region can be ascribed to a rigid wall boundary condition in a shallow water model, as shown by Jiang[31] and Yang[5]. Such a method can be used whenever the flow is symmetric across the track of the ship, as when a vessel travels along a straight line in open waters or in the middle of a channel, but can not be used for asymmetric problems, such as a ship traveling near one side wall in a channel.

2.4.1 Pressure disturbance

The problem of ascribing a certain hull shape to a particular pressure disturbance is made more complicated if a steady state is not attained, as is the case with near critical speed or if the velocity of the pressure disturbance changes with time. The surface displacement near the pressure disturbance depends on both the shape and the speed of the disturbance. In the near critical regime, nonlinear effects may also be important.

One effect which may seem counter-intuitive occurs in models with one horizontal dimension (1HD) when a pressure disturbance is moving at large supercritical speeds. in such a case the free surface displacement forms a hump of positive amplitude at the location of the pressure disturbance. An example is shown in figure 2.3 for Froude number $F_h = 1.4$, where the blue line is the surface displacement and the red line is the pressure disturbance.

In order to explain this phenomenon, we consider Bernoulli's equation,

$$\frac{1}{2}\left|\frac{\partial \Phi'}{\partial x'}\right|^2 + gz' + \frac{p'}{\rho} = \text{constant along a streamline},$$

which is valid for an inviscid, steady, barotropic flow. The flow is steady in a coordinate system that follows the pressure disturbance, which moves with the

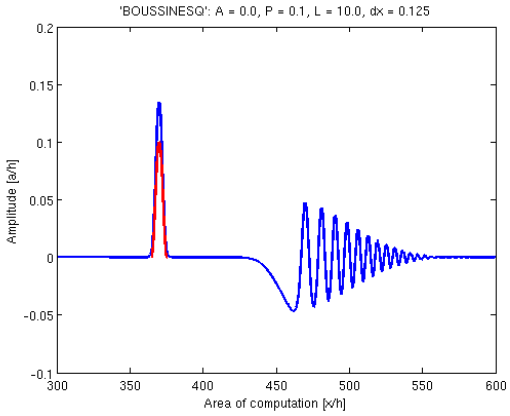

Figure 2.3: Example of a 1HD supercritical wave pattern

speed $u_0' = \partial\Phi_0'/\partial x'$. The free surface is a streamline for the flow, and we may equate conditions near the pressure disturbance with conditions far upstream or downstream from the disturbance

$$\frac{1}{2}\left|\frac{\partial\Phi'}{\partial x'}\right|^2 + gh' + \frac{p'}{\rho} = \frac{1}{2}\left|\frac{\partial\Phi_0'}{\partial x'}\right|^2 + gh_0\,, \tag{2.18}$$

where h_0 is the equilibrium depth and $h' = h_0 + \zeta$. Because of the continuity equation, we also have

$$\frac{\partial\Phi'}{\partial x'}h' = \frac{\partial\Phi_0'}{\partial x'}h_0 = u_0'h_0\,. \tag{2.19}$$

By combining equations (2.18) and (2.19), and recognizing that $F_h^2 = u_0'^2/gh_0$, we find

$$\frac{F_h^2}{2}\left(\frac{1+h}{h^2}\right)(1-h) - (1-h) = -p\,. \tag{2.20}$$

For small amplitude waves we have $(1+h)/h^2 \approx 2$, which gives us an approximation for equation (2.20) on the form

$$F_h^2(1-h) - (1-h) = -p\,,$$

which can be re-written as

$$(1-h) = \frac{p}{1-F_h^2}\,. \tag{2.21}$$

From equation 2.21 we see that the sign of $1-h$ changes depending on whether F_h is subcritical ($F_h < 1$) or supercritical ($F_h > 1$). We must emphasize that this result is valid for the 1HD case, which corresponds to a 2HD case of a pressure disturbance of infinite width propagating in an unbounded fluid.

Chapter 3

Numerical models

3.1 Grids for numerical models

While the mathematical model consists of partial differential equations which are defined for variables that are continuous in space and time, the numerical model must be solved for a finite number of points in space, and be integrated forward in time by discrete time steps. For numerical models based on finite differences, it is often convenient to apply computational grids with grid points distributed in a uniform pattern, with a constant distance between neighboring grid points. Since we are solving equations with only two spatial dimensions, we will only consider grids for surfaces in this section.

Most finite difference models which are discretized on regular grids, use rectangles (or hexahedrals in 3D) as the basic geometrical form. In the COULWAVE model, all the dependent variables are made available on a common set of grid points, located in the corners of the rectangles. This configuration corresponds to the so-called "Arakawa A-grid" (or just the A-grid), shown in figure 3.1(a), where u and v are the velocity components in the i and j direction, respectively, and h is some physical condition (water depth, density, temperature) we wish to describe.

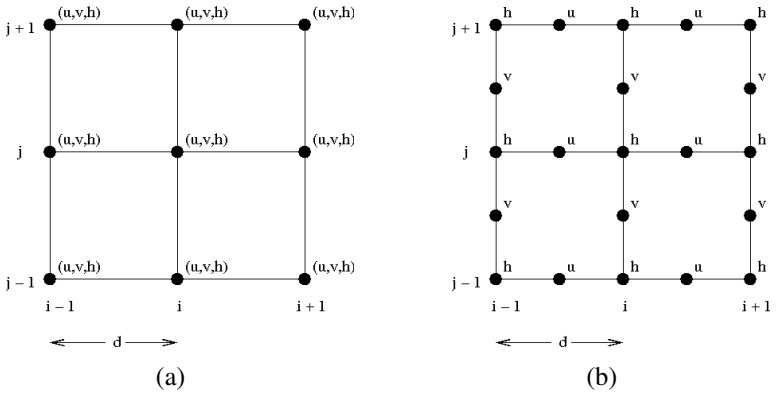

Figure 3.1: Arakawa A-grid and C-grid configurations.

Staggered grids can be constructed by specifying the dependent variables in different points, as in the C-grid shown in figure 3.1(b). Whenever we approximate the solution of a set of differential equations with a set of finite difference equations discretized on a grid, we are likely to find spurious effects which depend on the grid and not on the physical problem we are trying to solve. Different grid configurations tend to enhance or suppress different types of numerical errors, which must be taken into account when researchers develop numerical methods for a particular problem.

A general problem with rectangular grids is that they are anisotropic, and this can often cause a signal to propagate at a different speed along the grid axes than

along a diagonal axis. This problem can usually be mitigated by reducing the size of the grid, but there may be cases where this is not a practical solution. An alternative solution is to use hexagons instead of rectangles when constructing the grid. Because regular hexagons are less anisotropic than rectangles, hexagonal grids tend to induce less systematic errors then rectangular grids of similar size. Hexagonal grids have been applied by Sadourny et al.[32] and Williamson[33], and has since enjoyed some popularity in models for global atmospheric processes, because the sphere of the globe can be covered by a so-called icosahedral-hexagonal grid with nearly uniform hexagons.

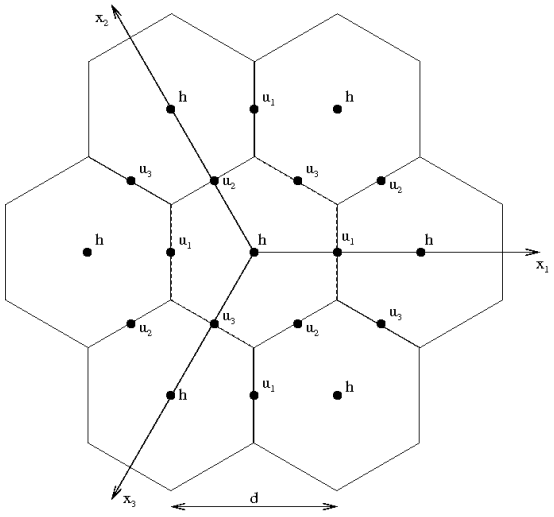

Figure 3.2: The HC-grid.

One type of hexagonal grid is the HC-grid (Hexagonal C-grid), shown in figure 3.2. This particular grid is formulated in terms of three horizontal axes, which means that one of the spatial variables can be written in terms of the other two. Details about the grid constructions can be found in appendix A.2. Not all hexagonal grids are formulated in terms of three spatial variables (see Ničković et al.[34] for an overview of different formulations), but this formulation preserves the symmetry of the problem as it is written with respect to a Cartesian coordinate system.

The *Lax-Richtmeyer equivalence theorem* guarantees that the numerical approximation to a set of linear differential equations with constant coefficient converges to the true solution if the approximate equations are consistent, i.e. approaches the partial differential equations as $\Delta x, \Delta t \to 0$, and the numerical scheme is stable, i.e. there is an upper limit to the errors introduced by roundoff. In paper D we examine the stability of numerical schemes for the shallow water equations discretized on a hexagonal grid. The growth of the numerical errors are related to an improper handling of depth variation in the water basin, and we show that a

stable numerical scheme can be constructed by choosing suitable weights on the Coriolis terms.

Although it is possible to discretize the Boussinesq equations on a hexagonal grid, we have not implemented such a model. This is partly because we have used an existing model, COULWAVE, for simulations in 2HD. As seen in section 2.2.2, the Boussinesq equations with improved dispersive properties perform well when compared to the linear solution, and further improvement is possible if higher order terms are retained in the equations. This reduces the incentive for using hexagonal grids with these equations, although there will still be significant errors in propagation speed for waves with short wave lengths.

3.2 Finite difference schemes for Boussinesq equations

The numerical models which have been employed in the papers are all based on finite difference schemes. As the basic theory of finite difference schemes for partial differential equations is textbook material (see e.g. Thomas[35]), this is not treated here. Because of the wide range of formulations used for the Boussinesq equations, several different numerical schemes have been proposed (see e.g. Peregrine[13, 13], Pedersen[36], Nwogu[14], Wei et al.[37]).

The numerical scheme used in paper A is similar to the scheme proposed by Pedersen[36]. The spatial differences are calculated using central differences of second-order accuracy. By discretizing the equations on a grid which is staggered both in space and time, updating of the velocity potential and surface elevation requires solving two tridiagonal matrices for each time step.

As mentioned earlier, the COULWAVE model which is used in papers B and C, is discretized using the unstaggered A-grid lattice. The spatial derivatives which occurs in the first-order terms are discretized to fourth-order accuracy by using standard five-point finite differencing, while the spatial derivatives occurring in the dispersive terms are differenced only to second-order accuracy. For the time stepping procedure, the fourth-order Adams-Bashforth-Moulton predictor-corrector scheme is employed. The corrector step is iterated until the error between two successive results for each of the three dependent variables u, v, and ζ reaches a required limit, which is typically fixed at $1.0 \cdot 10^{-4}$. By using methods with high order of accuracy for the first-order spatial derivatives and the temporal derivatives, we ensure that the truncation error terms are of a higher order than the dispersive terms in the equations.

3.3 Boundary conditions

Boundary conditions must be specified in order to have a well posed problem. For the papers presented in this thesis, we assume either that the lateral boundary is a solid wall that reflects the wave, or that the wave is absorbed at the boundary.

The solid boundary condition requires that the velocity component normal to the boundary is zero, i.e. that $\bar{\mathbf{u}} \cdot \bar{\mathbf{n}} = 0$ on the boundary, where $\bar{\mathbf{n}}$ is the normal vector to the boundary. This condition does not place any restrictions on the tangential velocity component, which must be determined by a separate boundary condition. In reality, fluid particles located on a solid boundary are stationary, which is expressed by the no-slip condition $\bar{\mathbf{u}} = 0$ on the boundary. As fluid in the core region of the flow usually have non-zero velocity, a strong shear flow develops close to the boundary, which is often difficult to handle in numerical models. In order to avoid this problem, many models use the free-slip condition $\partial\bar{\mathbf{u}}/\partial\bar{\mathbf{n}} = 0$, which restricts only the shear of the tangential velocity. The free-slip condition for solid boundaries is used in the COULWAVE model.

The absorbing boundary condition is constructed by introducing *sponge layers* extending over a certain width, starting from the boundary of the computational domain, where the solid boundary condition is applied. Inside the sponge layer, the flow is gradually relaxed toward the desired boundary condition by a smooth function. In the COULWAVE model, the sponge layer is used to damp waves propagating towards the boundary. In other models sponge layers may be used to relax the flow towards some external conditions, as seen for instance in ocean models where relaxation towards climatological values is often used for open boundaries.

3.3.1 The bottom boundary layer

The drag induced on the flow due to interaction with solid boundaries may be important for many applications. The effect of a no-slip boundary condition may be analyzed by assuming viscous effects are significant only within a boundary layer close to the solid surface, as outlined in appendix A.3. Matching the bottom boundary lay solution to the flow in the core region can be accomplished by modifying the bottom boundary conditions in the derivation of the Boussinesq equations. This introduces into the equations a term which contains a convolution integral in time (see Liu and Orfila[38]). Although it is not difficult to calculate the value of this integral in principle, it is very computationally demanding for practical applications. Computing the value of this integral in a straight forward manner requires that we know the entire history of the flow in each of the grid points. Not only do we have to store all these value, but for each time step we have to integrate over all spatial nodes and all time steps. If we are to use the

boundary layer approach for large scale simulations, there is clearly a need for finding a good estimate of the convolution integral by a less computationally demanding method. A procedure for finding such an estimate is presented paper C.

Chapter 4

Summary and future work

Papers A and B explore the generation of waves under some specific conditions which may be of importance for HSC operations in shallow waters. This line of investigation may be extended further. For instance, in the accident report following the swamping of the angling vessel ”Purdy”[8] it was suggested that wave focusing due to a change in the course of the HSC could have contributed to the accident. The modeling tools discussed in this thesis could be used to explore a similar scenario by having the wave generating disturbance move along a curved path.

When working with numerical models, one must always question whether the end result corresponds to a true solution of the physical problem, or if the result is an artifact created by conditions inherent in the mathematical or numerical model itself. The result could be checked against data from experiments or field measurements if these are available, or against the result from a mathematical or numerical model which is considered to be more accurate or reliable. For the test cases discussed in papers A and B we have not had any data available for comparison. It would be of interest to compare the results in these papers with results from a more accurate model which is not based on the shallow water approximation.

If we want to use Boussinesq equations to study wave generation due to a particular hull shape, we need a more accurate description of the near ship flow. One possibility would be to apply the slender body theory mentioned in section 2.4, which has been used successfully by other researchers.

Paper C explores the viscous effects due to a transient long wave. This theory can be used for waves generated by a vessel in shallow water, as was demonstrated in one of the examples in the paper, but could also be used when modeling other transient phenomena, such as dam break problems or gravity plumes. The theory can be extended to include flow near sidewall boundaries in a channel, but has so far only been implemented in a width averaged model formulation (see Liu et al.[39]).

Paper D use hexagonal grids for shallow water equations, and explores issues related to stability by examining the propagation matrix. As mentioned in section 3.1, it is possible to formulate the Boussinesq equations it terms of the hexagonal coordinate system, and it would be interesting to examine if this formulation improved results for waves of intermediate wave length. The stability analysis method used in paper D can be applied to other grids and model equations (see discussion in Espelid et al.[40]).

Appendix A

Appendix

A.1 Derivation of the Boussinesq equations

In this section, we briefly outline how we can derive the Boussinesq equations from the primitive equations (2.1) to (2.5), following the procedure used by Madsen and Schäffer[16]. This procedure is based on the velocity potential, which is defined by

$$u' = \frac{\partial \Phi'}{\partial x'}, \qquad v' = \frac{\partial \Phi'}{\partial y'}, \qquad w' = \frac{\partial \Phi'}{\partial z'}.$$

The non-dimensional variables are defined as

$$(x,y) = \frac{(x',y')}{l'_0}, \qquad z = \frac{z'}{h'_0}, \qquad h = \frac{h'}{h'_0}, \qquad t = \frac{\sqrt{gh'_0}}{l'_0}t',$$
$$\Phi = \frac{h'_0}{a'_0 l'_0 \sqrt{gh'_0}}\Phi' \qquad \zeta = \frac{\zeta'}{a'_0}, \qquad p = \frac{p'}{\rho g a'_0},$$

and this gives us the governing equations on the form

$$\Phi_{zz} + \mu^2 \nabla^2 \Phi = 0, \qquad -h < z < \varepsilon\zeta, \tag{A.1}$$

$$\frac{1}{\mu^2}\Phi_z + \nabla h \cdot \nabla \Phi = 0, \qquad z = -h, \tag{A.2}$$

$$\Phi_t + \zeta + p + \frac{1}{2}\varepsilon(\nabla\Phi)^2 + \frac{\varepsilon}{2\mu^2}(\Phi_z)^2 = 0, \qquad z = \varepsilon\zeta, \tag{A.3}$$

$$-\frac{1}{\mu^2}\Phi_z + \zeta_t + \varepsilon\nabla\zeta \cdot \nabla\Phi = 0, \qquad z = \varepsilon\zeta. \tag{A.4}$$

Power series expansion

We now assume that the solution can be expressed as a power series in z, according to

$$\Phi(x,y,z,t) = \sum_{n=0}^{\infty} z^n \Phi^{(n)}(x,y,t)\,. \tag{A.5}$$

Using this expansion in the Laplace equation (A.1), we find

$$\Phi^{(n+2)} = -\mu^2 \frac{\nabla^2 \Phi^{(n)}}{(n+1)(n+2)}\,, \qquad n = 1,2,3,\ldots\,,$$

and the power series solution (A.5) can now be expressed as

$$\Phi(x,y,z,t) = \sum_{n=0}^{\infty} (-1)^n \mu^{2n} \left(\frac{z^{2n}}{(2n)!} \nabla^{2n} \Phi^{(0)} + \frac{z^{2n+1}}{(2n+1)!} \nabla^{2n} \Phi^{(1)} \right). \tag{A.6}$$

We may regain the formulation in terms of velocities by

$$\mathbf{u}(x,y,z,t) = \sum_{n=0}^{\infty} (-1)^n \left(\frac{z^{2n}}{(2n)!} \mu^{2n} \nabla(\nabla^{2n-2}(\nabla\cdot\hat{\mathbf{u}})) + \frac{z^{2n+1}}{(2n+1)!} \mu^{2n+2} \nabla(\nabla^{2n}\hat{w}) \right),$$

$$w(x,y,z,t) = \sum_{n=0}^{\infty} (-1)^n \left(-\frac{z^{2n+1}}{(2n+1)!} \mu^{2n+2} \nabla^{2n}(\nabla\cdot\hat{\mathbf{u}}) + \frac{z^{2n}}{(2n)!} \mu^{2n+2} \nabla^{2n}\hat{w} \right),$$

where we have defined

$$\hat{\mathbf{u}} \equiv \nabla\Phi^{(0)}\,, \qquad \hat{w} \equiv \frac{1}{\mu^2}\Phi^{(1)}\,.$$

It is easy to verify that

$$\mathbf{u}(x,y,0,t) = \hat{\mathbf{u}}\,, \qquad w(x,y,0,t) = \mu^2\hat{w}\,,$$

by setting $z = 0$ in the above equations.

The kinematic bottom boundary condition

Replacing Φ with the series expression (A.6), we find that the kinematic bottom boundary condition (A.2) becomes

$$\sum_{n=0}^{\infty} (-1)^n \left(\mu^{2n} \frac{h^{2n+1}}{(2n+1)!} \nabla^{2n}(\nabla\cdot\hat{\mathbf{u}}) + \mu^{2n} \frac{h^{2n}}{(2n)!} \nabla^{2n}\hat{w} \right)$$
$$+\nabla h \cdot \sum_{n=0}^{\infty} (-1)^n \left(\mu^{2n} \frac{h^{2n}}{(2n)!} \nabla(\nabla^{2n-2}(\nabla\cdot\hat{\mathbf{u}})) - \mu^{2n+2} \frac{h^{2n+1}}{(2n+1)!} \nabla(\nabla^{2n}\hat{w}) \right) = 0\,.$$

Using the identity

$$\hat{w} = \sum_{n=0}^{\infty} (-1)^n \mu^{2n} \left(\frac{h^{2n}}{(2n)!} \nabla^{2n} \hat{w} + \mu^2 \frac{h^{2n+2}}{(2n+2)!} \nabla^2 (\nabla^{2n} \hat{w}) \right),$$

we write the above equation on the equivalent form

$$\hat{w} + \sum_{n=0}^{\infty} (-1)^n \mu^{2n} \nabla \cdot \left(\frac{h^{2n+1}}{(2n+1)!} \nabla (\nabla^{2n-2} (\nabla \cdot \hat{\mathbf{u}})) \right.$$
$$\left. - \mu^2 \frac{h^{2n+2}}{(2n+2)!} \nabla (\nabla^{2n} \hat{w}) \right) = 0 .$$

So far we have proceeded without making any assumptions concerning the magnitude of the parameters μ and ε. Hereafter we assume that $\mu \ll 1$, and introduce the series expansion for $\hat{w}$ as

$$\hat{w}(x,y,t) = \sum_{m=0}^{\infty} \mu^{2m} w^{(m)}(x,y,t) .$$

Replacing the series expansion for $\hat{w}$ in the above equation gives us two single summation series and one double summation series. We replace m and n with p in the single summation series and replace m with $p-n-1$ in the double summation series. Having assumed $\mu \ll 1$, all elements of equal power in μ must sum to zero, which gives us

$$w^{(p)} = \frac{(-1)^{p+1}}{(2p+1)!} \nabla \cdot [h^{2p+1} \nabla (\nabla^{2p-2} (\nabla \cdot \hat{\mathbf{u}}))]$$
$$+ \sum_{n=0}^{p-1} \frac{(-1)^n}{(2n+2)!} \nabla \cdot [h^{2n+2} \nabla (\nabla^{2n} w^{(p-n-1)})] .$$

We are now in a position where we can express $\hat{w}$ in terms of $\hat{\mathbf{u}}$ to any order of μ. The explicit expression including the first three terms in p, is

$$\begin{aligned} \hat{w}(x,y,t) = & -\nabla \cdot (h\hat{\mathbf{u}}) + \mu^2 \nabla \cdot [\tfrac{1}{6} h^3 \nabla (\nabla \cdot \hat{\mathbf{u}}) - \tfrac{1}{2} h^2 \nabla (\nabla \cdot (h\hat{\mathbf{u}}))] \\ & + \mu^4 \nabla \cdot [\tfrac{1}{24} h^4 \nabla (\nabla^2 (\nabla \cdot (h\hat{\mathbf{u}}))) - \tfrac{1}{120} h^5 \nabla (\nabla^2 (\nabla \cdot \hat{\mathbf{u}})) \\ & + \tfrac{1}{2} h^2 \nabla (\nabla \cdot (\tfrac{1}{6} h^3 \nabla (\nabla \cdot \hat{\mathbf{u}}) - \tfrac{1}{2} h^2 \nabla (\nabla \cdot (h\hat{\mathbf{u}}))))] + O(\mu^6) \end{aligned}$$

The kinematic boundary condition at the free surface

We define velocities at the free surface by

$$\tilde{\mathbf{u}} \equiv (\nabla \Phi)_{z=\varepsilon\zeta} , \qquad \tilde{w} \equiv \frac{1}{\mu^2} (\Phi_z)_{z=\varepsilon\zeta} ,$$

and write the kinematic free boundary condition (A.4) as

$$\zeta_t - \tilde{w} + \varepsilon \nabla\zeta \cdot \tilde{\mathbf{u}} = 0\,.$$

Using the series expansion of Φ, we find series expansions for $\tilde{\mathbf{u}}$ and $\tilde{w}$ in terms of $\hat{\mathbf{u}}$ and $\hat{w}$,

$$\tilde{\mathbf{u}} = \sum_{n=0}^{\infty} (-1)^n \mu^{2n} \varepsilon^{2n} \left(\frac{\zeta^{2n}}{(2n)!} \nabla(\nabla^{2n-2}(\nabla\cdot\hat{\mathbf{u}})) + \mu^2 \varepsilon \frac{\zeta^{2n+1}}{(2n+1)!} \nabla(\nabla^{2n}\hat{w}) \right),$$

$$\tilde{w} = \hat{w} - \sum_{n=0}^{\infty} (-1)^n \mu^{2n} \varepsilon^{2n+1} \left(\frac{\zeta^{2n+1}}{(2n)!} \nabla^{2n}(\nabla\cdot\hat{\mathbf{u}}) + \mu^2 \varepsilon \frac{\zeta^{2n+2}}{(2n+2)!} \nabla\cdot(\nabla(\nabla^{2n}\hat{w})) \right).$$

This gives us the kinematic free boundary condition

$$\zeta_t - \hat{w} + \sum_{n=0}^{\infty} (-1)^n \mu^{2n} \varepsilon^{2n+1} \nabla\cdot \left(\frac{\zeta^{2n+1}}{(2n+1)!} \nabla(\nabla^{2n-2}(\nabla\cdot\hat{\mathbf{u}})) \right.$$
$$\left. \mu^2 \varepsilon \frac{\zeta^{2n+2}}{(2n+2)!} \nabla(\nabla^{2n}\hat{w}) \right) = 0\,,$$

which is valid for arbitrary values of ζ and μ. Using the polynomial expression for $\hat{w}$ in terms of $\hat{\mathbf{u}}$ (assuming $\mu \ll 1$), we find

$$\begin{aligned}
\zeta_t + \nabla\cdot\{&(\varepsilon\zeta + h)\hat{\mathbf{u}} - \mu^2[\tfrac{1}{2}(\varepsilon^2\zeta^2 - h^2)\nabla(\nabla\cdot(h\hat{\mathbf{u}})) + \tfrac{1}{6}(\varepsilon^3\zeta^3 + h^3)\nabla(\nabla\cdot\hat{\mathbf{u}})] \\
&+ \mu^4[\tfrac{1}{2}(\varepsilon^2\zeta^2 - h^2)\nabla(\nabla\cdot(\tfrac{1}{6}h^3\nabla(\nabla\cdot\hat{\mathbf{u}}) - \tfrac{1}{2}h^2\nabla(\nabla\cdot(h\hat{\mathbf{u}})))) \\
&+ \tfrac{1}{24}(\varepsilon^4\zeta^4 - h^4)\nabla(\nabla^2(\nabla\cdot(h\hat{\mathbf{u}}))) + \tfrac{1}{120}(\varepsilon^5\zeta^5 + h^5)\nabla(\nabla^2(\nabla\cdot\hat{\mathbf{u}}))]\} \\
&= O(\mu^6)
\end{aligned}$$

The dynamic boundary condition

The dynamic free surface boundary condition (A.3) may be treated in different ways. When deriving the Boussinesq equations, it is customary to apply a procedure which requires spatial and temporal derivatives of Φ to be calculated before z is replaced by $\varepsilon\zeta$ in the series expansions. This ensures that the equation derived from the dynamic boundary condition does not include temporal derivatives of ζ. Formulations have been constructed where temporal derivatives of ζ are included in both Boussinesq equations, but in this case we will follow the traditional procedure.

We start by defining

$$\Phi_t^* \equiv (\Phi_t)_{z=\varepsilon\zeta}\,, \qquad \mathbf{V}_t^* \equiv \nabla(\Phi_t^*)\,,$$

and write the dynamic boundary condition as

$$\Phi_t^* + \zeta + p + \varepsilon \frac{\tilde{\mathbf{u}} \cdot \tilde{\mathbf{u}}}{2} + \varepsilon \mu^2 \frac{\tilde{w}^2}{2} = 0 \,.$$

Differentiating with respect to horizontal spatial dimensions, we find

$$\mathbf{V}_t^* + \nabla \zeta + \nabla p + \nabla \left(\varepsilon \frac{\tilde{\mathbf{u}} \cdot \tilde{\mathbf{u}}}{2} + \varepsilon \mu^2 \frac{\tilde{w}^2}{2} \right) = 0 \,.$$

We have already obtained series expansions for $\tilde{\mathbf{u}}$ and $\tilde{w}$, and the series expansion for $\mathbf{V}_t^*$ is given as

$$\mathbf{V}_t^* = \sum_{n=0}^{\infty} (-1)^n \mu^{2n} \varepsilon^{2n} \nabla \left(\frac{\zeta^{2n}}{(2n)!} \nabla^{2n-2} (\nabla \cdot \hat{\mathbf{u}}_t) + \mu^2 \varepsilon \frac{\zeta^{2n+1}}{(2n+1)!} \nabla^{2n} \hat{w}_t \right) .$$

This establishes the Boussinesq equations in terms of the velocity at still water level. Other formulations may use the depth-averaged velocity or the velocity at an arbitrary z-level. Any such formulation may be derived by using the above formulations, and replace the wanted velocity component for $\hat{\mathbf{u}}$ by successive replacements in the series expansion of $\mathbf{u}(x, y, z, t)$.

A.2 Properties of the hexagonal coordinate system

Equations formulated in a Cartesian coordinate system (x,y) can be formulated in the HC-coordinate system (x_1,x_2,x_3) by the transformation

$$x_1 = x, \quad x_2 = -\frac{1}{2}x + \frac{\sqrt{3}}{2}y, \quad x_3 = -\frac{1}{2}x - \frac{\sqrt{3}}{2}y.$$

This system is over-determined, so one component can be written in terms of the other two. If for instance the velocity $u = (u_1,u_2,u_3)$, is defined in the point $p = (p_1,p_2,p_3)$, we have the relation

$$u_1(p) + u_2(p) + u_3(p) = 0\,,$$

between the velocity components. Furthermore, the length of a vector in the HC-coordinate system can be related to the length of the corresponding vector in the Cartesian coordinate system through the relation

$$u_1^2(p) + u_2^2(p) + u_3^2(p) = \frac{3}{2}(u^2(p) + v^2(p))$$

Further details about the construction and basic properties of this grid can be found in articles by Sadourny and Morel[41], Ničković[42], and Ničković et al.[34].

The linearized shallow water equations with Coriolis forcing, is written in component form in a Cartesian coordinate system as

$$\begin{aligned}
\frac{\partial u}{\partial t} - fv + g\frac{\partial h}{\partial x} &= 0\,,\\
\frac{\partial v}{\partial t} + fu + g\frac{\partial h}{\partial y} &= 0\,,\\
\frac{\partial h}{\partial t} + H_0\left(\frac{\partial u}{\partial x} + \frac{\partial v}{\partial y}\right) &= 0\,,
\end{aligned}$$

where the depth H is written as $H(x,y,t) = H_0(x,y) + h(x,y,t)$. Transforming this equation on the HC-coordinate system, we formulate the equations

$$\begin{aligned}
\frac{\partial u_1}{\partial t} - \frac{f}{\sqrt{3}}(u_2 - u_3) + g\frac{\partial h}{\partial x_1} &= 0\,,\\
\frac{\partial u_2}{\partial t} - \frac{f}{\sqrt{3}}(u_3 - u_1) + g\frac{\partial h}{\partial x_2} &= 0\,,\\
\frac{\partial u_3}{\partial t} - \frac{f}{\sqrt{3}}(u_1 - u_2) + g\frac{\partial h}{\partial x_3} &= 0\,,\\
\frac{\partial h}{\partial t} + \frac{2}{3}H_0\left(\frac{\partial u_1}{\partial x_1} + \frac{\partial u_2}{\partial x_2} + \frac{\partial u_3}{\partial x_3}\right) &= 0\,.
\end{aligned}$$

The improvement with respect to isotropic properties can be seen in figure A.1, where the phase speed of the shallow water wave is plotted relative to the analytical phase speed $c = \sqrt{gh}$. The phase speed for the numerical solution is found by discretizing the equations in space only, and inserting a wave solution on the form $\phi = \phi_0 \exp(i(\alpha m\Delta x + \beta n\delta y - \nu t))$. The phase speeds for the wave in the C-grid is

$$c_C = \frac{\nu_C}{\sqrt{\alpha^2+\beta^2}} = \frac{2\sqrt{gh}}{d\sqrt{\alpha^2+\beta^2}}\left[\sin^2\left(\frac{\alpha d}{2}\right)+\sin^2\left(\frac{\beta d}{2}\right)\right]^{\frac{1}{2}},$$

and the phase speed for the HC-grid is

$$\begin{aligned} c_{HC} &= \frac{\nu_{HC}}{\sqrt{\alpha^2+\beta^2}} \\ &= \left[\left(\frac{8gh}{3d^2(\alpha^2+\beta^2)}\right)\left(\sin^2(2a)+\sin^2(a-b)+\sin^2(a+b)\right)\right]^{\frac{1}{2}}, \end{aligned}$$

where $a = \alpha d/4$, and $b = \sqrt{3}\beta d/4$.

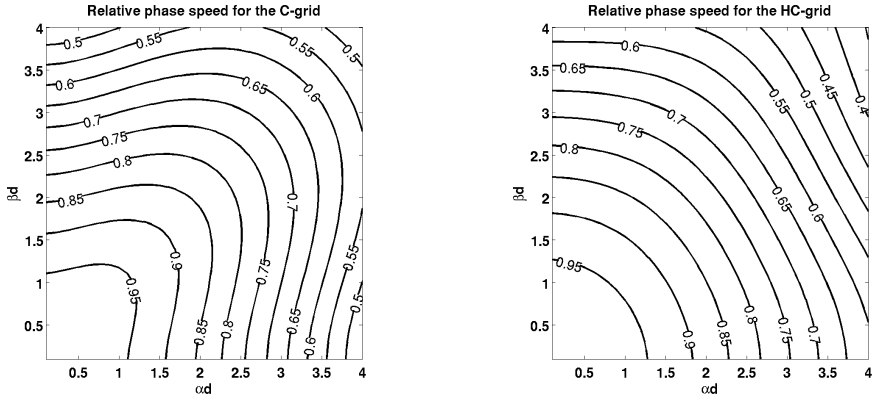

(a) (b)

Figure A.1: Relative phase speed for the C-grid and HC-grid.

The frequency of the gravity-inertia waves is

$$\left(\frac{\omega}{f}\right)^2 = 1 + R_D^2(k^2+l^2),$$

where $R_D = \sqrt{gH_0}/f$ is the Rossby radius. Results for the C-grid and HC-grid are

$$\left(\frac{\nu_C}{f}\right)^2 = \cos^2\left(\frac{\alpha d}{2}\right)\cos^2\left(\frac{\beta d}{2}\right) + \frac{4R_D^2}{d^2}\left(\sin^2\left(\frac{\alpha d}{2}\right)+\sin^2\left(\frac{\beta d}{2}\right)\right),$$

and

$$\left(\frac{\nu_{HC}}{f}\right)^4 + B\left(\frac{\nu_{HC}}{f}\right)^2 + C = 0\,,$$

$$\begin{aligned} B =& \frac{4R_D^2}{3d^2}\left[\cos(4a)+\cos(2a-2b)+\cos(2a+2b)-3\right] \\ & -\frac{1}{6}\left[\cos(4a)+\cos(2a-2b)+\cos(2a+2b)+3\right]\,, \\ C =& \frac{8R_D^2}{9d^2}\left[\cos(2a)-\cos(2b)\right]^2\sin^2(2a)\,. \end{aligned}$$

The expression for B is slightly different from the expression presented in [34], due to a misprint in that paper (confirmed by Ničković in private communication).

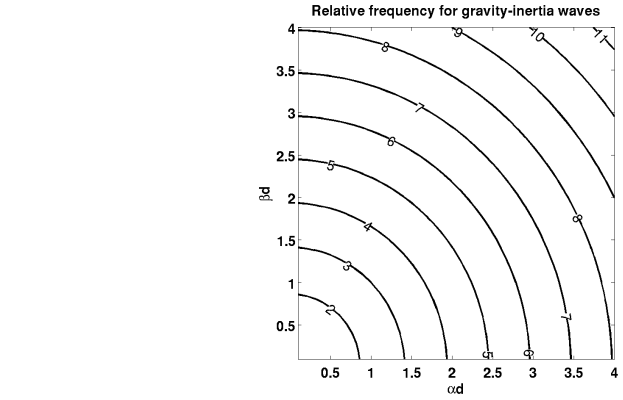

(a)

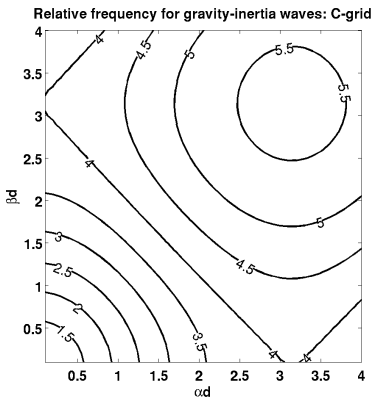

(b)

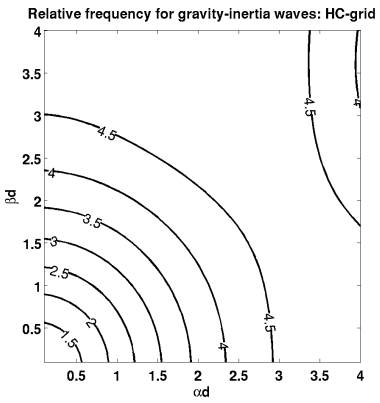

(c)

Figure A.2: Relative wave frequency for inertia-gravity waves.

A.3 Diffusion in the Bottom Boundary Layer

Diffusion on a semi-infinite rod is governed by the PDE

$$\frac{\partial u}{\partial t} = k\frac{\partial^2 u}{\partial x^2}, \qquad 0 < x < \infty,$$

with boundary conditions

$$u(0,t) = g(t) \qquad \text{and} \qquad u(\infty,t) = 0, \qquad t > 0,$$

and the initial condition

$$u(x,0) = h(x).$$

The solution to this type of problems can be found in text-books on PDEs (see e.g. Mei[43]). We use the Fourier sine transform

$$\hat{u}(\xi,t) = \int_0^\infty u(x,t)\sin(\xi x)\,dx,$$

which transforms the above PDE to the ordinary differential equation

$$\frac{d\hat{u}}{dt} + k\xi^2\hat{u} = k\xi g(t), \qquad t > 0,$$

with the initial condition

$$\hat{u}(\xi,0) = \hat{h}(\xi) = \int_0^\infty h(x)\sin(\xi x)\,dx.$$

The ODE for the transformed problem has the general solution

$$\hat{u}(\xi,t) = \hat{h}e^{-k\xi^2 t} + k\xi\int_0^t g(\tau)e^{-k\xi^2(t-\tau)}\,d\tau.$$

Assuming zero initial condition $h = \hat{h} = 0$, the solution in physical space is found by using the inverse Fourier sine transform, giving

$$\begin{aligned}
u(x,t) &= \frac{2k}{\pi}\int_0^\infty \xi\sin(\xi x)\int_0^t g(\tau)e^{-k\xi^2(t-\tau)}\,d\tau\,d\xi \\
&= \frac{2k}{\pi}\int_0^t g(\tau)\int_0^\infty \xi\sin(\xi x)e^{-k\xi^2(t-\tau)}\,d\xi\,d\tau \\
&= \frac{2k}{\pi}\int_0^t g(\tau)\left(-\frac{\partial}{\partial x}\int_0^\infty \cos(\xi x)e^{-k\xi^2(t-\tau)}\,d\xi\right)d\tau \\
&= \frac{2k}{\pi}\int_0^t \frac{g(\tau)}{\sqrt{k(t-\tau)}}\left(-\frac{\partial}{\partial x}\int_0^\infty \cos(\mu z)e^{-z^2}\,dz\right)d\tau
\end{aligned}$$

where $z^2 = k\xi^2(t-\tau)$ and $\mu = x/\sqrt{k(t-\tau)}$.

We solve the inner integral

$$I(\mu) = \int_0^\infty \cos(\mu z) e^{-z^2}\, dz$$

by first taking the derivative

$$\begin{aligned}\frac{dI}{d\mu} &= -\int_0^\infty z\sin(\mu z) e^{-z^2}\, dz = \frac{1}{2}\int_0^\infty \sin(\mu z) d(e^{-z^2}) \\ &= \left[\frac{1}{2}e^{-z^2}\sin(\mu z)\right]_0^\infty - \frac{1}{2}\mu\int_0^\infty \cos(\mu z) e^{-z^2}\, dz \\ &= -\frac{1}{2}\mu I(\mu)\,.\end{aligned}$$

This ODE in $I(\mu)$ has initial condition

$$I(0) = \int_0^\infty e^{-z^2}\, dz = \frac{\sqrt{\pi}}{2}\,,$$

which determines the solution

$$I(\mu) = I(0)e^{-\frac{\mu^2}{4}} = \frac{\sqrt{\pi}}{2}e^{-\frac{\mu^2}{4}}\,.$$

Returning to the original problem, we find

$$\begin{aligned}u(x,t) &= 2k\int_0^t \frac{g(\tau)}{\sqrt{4\pi k(t-\tau)}}\left(-\frac{\partial}{\partial x}e^{-\frac{x^2}{4k(t-\tau)}}\right) d\tau \\ &= \frac{x}{\sqrt{4\pi k}}\int_0^t \frac{g(\tau)}{(t-\tau)^{\frac{3}{2}}} e^{-\frac{x^2}{4k(t-\tau)}}\, d\tau\end{aligned}$$

Bibliography

[1] O. M. Faltinsen, *Hydrodynamics of High-Speed Marine Vehicles*. Cambridge University Press, 2005. ISBN 0-521-84568-8.

[2] J. J. Stoker, *Water Waves*. Inerscience Publushers, Inc., 1957.

[3] R. Doyle, T. Whittaker, and B. Elsäßer, "A study of fast ferry wash in shallow water.," in *Proceedings FAST2001*, (Southampton), 2001.

[4] J. N. Newman, *Marine hydrodynamics*. The MIT Press, 1977. ISBN 0-262-14026-8.

[5] Q. Yang, *Wash and Wave Resistance of Ships in Finite Water Depth*. PhD thesis, NTNU Trondheim, 2002. ISBN 82-471-5427-7.

[6] S. Stumbo, K. Fox, and L. Elliot, "An assesment of wake wash reduction of fast ferries at supercritical froude numbers and optimised trim," in *Proceedings of the International Conference on Hydrodynamics of High Speed Craft*, (London), RINA, November 2000.

[7] K. E. Parnell and H. Kofoed-Hansen, "Wakes from large high-speed ferries in confined coastal waters: Management approaches with examples from new zealand and denmark," *Coastal Management*, vol. 29, pp. 217–237, 2001.

[8] "Report on the investigation of the man overboard fatality from angling boat purdy at shipwash bank, off harwich on 17 july 1999." Marine Accident Investigation Branch, 2000. Report No 17/2000.

[9] T. Soomere, "Fast ferry traffic as a quantitively new forcing factor of environmental processes in non-tidal sea areas: A case study in tallinn bay, baltic sea," *Environmental Fluid Mechanics*, vol. 5, pp. 293–323, 2005.

[10] S. Stumbo, K. Fox, F. Dvorak, and L. Elliot, "The prediction, measurement, and analysis of wake wash from marine vessels," *Marine Technology*, vol. 36, no. 4, pp. 248–260, 1999.

[11] P. K. Kundu, *Fluid Mechanics*. Academic Press, 1990. ISBN-0-12-428770-0.

[12] A. B. Kennedy, Q. Chen, J. T. Kirby, and R. A. Dalrymple, "Boussinesq modeling of wave transformation, breaking, and runup," *Journal of waterway, port, coastal, and ocean engineering*, vol. 126, no. 1, pp. 39–47, 2000.

[13] D. H. Peregrine, "Long waves on a beach," *Journal of Fluid Mechanics*, vol. 27, pp. 815–827, 1967.

[14] O. Nwogu, "Alternative form of boussinesq equations for nearshore wave propagation," *Journal of waterway, port, coastal, and ocean engineering*, vol. 119, no. 6, pp. 618–638, 1993.

[15] C. C. Mei, *The applied dynamics of ocean surface waves*. Wiley-Interscience, 1983. ISBN 0-471-06407-6.

[16] P. A. Madsen and H. A. Schäffer, "A review of boussinesq-type equations for surface gravity waves," in *Advances in Coastal and Ocean Engineering* (P. L.-F. Liu, ed.), vol. 5, pp. 1–94, World Scientific, Singapore, 1999. ISBN 981-02-3859-2.

[17] T. Y. Wu, "Long waves in ocean and coastal waters," *J. Eng. Mech. Div. ASCE*, vol. 107, pp. 501–522, 1981.

[18] G. Pedersen, "On the numerical solution of the boussinesq equations," research rep. in mechanics, University of Oslo, 1988.

[19] S. Lee, G. Y. Yates, and T. Y. Wu, "Experiments and analysis of upstream-advancing solitary waves generated by moving disturbances," *J. Fluid Mech.*, vol. 199, pp. 569–593, 1989.

[20] P. G. Drazin and R. S. Johnson, *Solitons: an introduction*. Cambridge University Press, 1989. ISBN-0-521-33655-4.

[21] F. Løvholt and G. Pedersen, "Instabilities of boussinesq models in non-uniform depth." Preprint submitted to Journal of Computational Physics, 2006.

[22] A. S. Peters, "Rotational and irrotational solitary waves in a channel with arbitrary cross-section," *Commun. pure appl. Math*, vol. 19, pp. 445–471, 1966.

[23] D. H. Peregrine, "Long waves in a uniform channel of arbitrary cross-section," *J. Fluid Mech.*, vol. 32, no. 2, pp. 353–365, 1968.

[24] D. H. Peregrine, "Solitary waves in trapezoidal channels," *J. Fluid Mech.*, vol. 35, no. 1, pp. 1–6, 1969.

[25] M. H. Teng and T. Y. Wu, "Nonlinear water waves in channels of arbitreary shape," *J. Fluid Mech.*, vol. 242, pp. 211–233, 1992.

[26] M. H. Teng and T. Y. Wu, "Evolution of long water waves in variable channels," *J. Fluid Mech.*, vol. 266, pp. 303–317, 1994.

[27] M. H. Teng and T. Y. Wu, "Effects of channel cross-sectional geometry on long wave generation and propagation," *Phys. Fluids*, vol. 9, no. 11, pp. 3368–3377, 1997.

[28] E. O. Tuck, D. C. Scullen, and L. Lazauskas, "Wave patterns and minimum wave resistance for high-speed vessels," in *Proceedings for the 24th Symposium on Naval Hydrodynamics*, (Fukuoka), 2002.

[29] J. H. Michell, "The wave-resistance of a ship," *Phil. Mag.*, vol. 45, 1898.

[30] E. O. Tuck, "Shallow-water flows past slender bodies," *J. Fluid Mech.*, vol. 26, no. 1, pp. 81–95, 1966.

[31] T. Jiang, "Investigation of waves generated by ships in shallow water," in *Proceedings for the 22nd Symposium on Naval Hydrodynamics*, (Washington D.C., USA), 1998.

[32] R. Sadourny, A. Arakawa, and Y. Mintz, "Integration of nondivergent barotropic velocity equation with an icosahedral-hexagonal grid for the sphere," *Mon. Wea. Rev.*, vol. 96, pp. 351–356, June 1968.

[33] D. Williamson, "Integration off the barotropic vorticity equation on a spherical geodesic grid," *Tellus XX*, vol. 4, pp. 642–653, 1968.

[34] S. Ničković, M. Gavrilov, and I. Tošić, "Geostrophic Adjustment on Hexagonal Grids," *Mon. Wea. Rev.*, vol. 130, pp. 668–683, March 2002.

[35] J. W. Thomas, *Numerical Partial Differential Equations: Finite Difference Methods*. Springer, 1995. ISBN-0-387-97999-9.

[36] G. Pedersen, "Three-dimensional wave patterns generated by moving disturbances at transcritical speeds," *J. Fluid Mech.*, vol. 196, pp. 39–63, 1988.

[37] G. Wei, J. T. Kirby, S. T. Grilli, and R. Subramanya, "A fully nonlinear boussinesq model for surface waves. part 1. highly nonlinear unsteady waves," *Journal of Fluid Mechanics*, vol. 294, pp. 71–92, 1995.

[38] P. L.-F. Liu and A. Orfila, "Viscous effects on transient long-wave propagation," *J. Fluid Mech.*, vol. 520, pp. 83–92, 2004.

[39] P. L.-F. Liu, G. Simorra, J. Vandever, and A. Orfila, "Experimental and numerical investigation of viscous effects on solitary waves propagation ain a wave tank," *Coastal Engineering*, vol. 53, no. 2-3, pp. 181–190, 2006.

[40] T. Espelid, J. Berntsen, and K. Barthel, "Conservation of energy for schemes applied to the propagation of shallow-water inertia-gravity waves in regions with varying depth," *Int. J. Numer. Meth. Engng.*, vol. 49, pp. 1521–1545, 2000.

[41] R. Sadourny and P. Morel, "A finite-difference approximation of the primitive equations for a hexagonal grid on a plane," *Mon. Wea. Rev.*, vol. 97, pp. 439–445, June 1969.

[42] S. Ničković, "On the use of hexagonal grids for simulation of atmospheric processes," *Beitr. Phys. Atmosph.*, vol. 67, pp. 103–107, May 1994.

[43] C. C. Mei, *Mathematical Analysis in Engineering*. Cambridge University Press, 1995. ISBN 0-521-46053-0.